Dynamics of a dinuclear system in charge-asymmetry coordinates: α decay, cluster radioactivity, and spontaneous fission

I. S. Rogov,[1,2] G. G. Adamian,[2] and N. V. Antonenko[2]
[1]*Tomsk Polytechnic University, 634050 Tomsk, Russia*
[2]*Joint Institute for Nuclear Research, 141980 Dubna, Russia*

(Received 18 May 2019; published 5 August 2019)

The possibility of application of the dinuclear system model to the simultaneous description of α decay, cluster radioactivity, and spontaneous fission is discussed. The half-lives of cluster decay and spontaneous fission for the nuclei ^{232,234,236}U, ^{236,238}Pu, ^{242}Cm, and ^{248}Cf are calculated within the same approach and compared with existing experimental data. The cluster radioactivity in the ^{248}Cf nucleus is predicted.

DOI: 10.1103/PhysRevC.100.024606

I. INTRODUCTION

After the emission of ^{14}C by ^{223}Ra was discovered [1,2], other cluster radioactivities have been observed. Nowadays, α decay, cluster radioactivity (CR), and spontaneous fission (SF) attract attention in connection with the studies of the structure of heavy and superheavy nuclei. One of the most challenging tasks is to describe the SF and CR processes in a single approach with the same parameters. While the SF results in the products with masses close to the half of the mass of mother nucleus, the CR produces quite asymmetric fragments. So, the CR can be considered as the superasymmetric fission [3–6]. The existing models of the CR are distinguished by means of calculation of preformation or spectroscopic factors S_L for cluster L. In the models with $S_L = 1$, the effect of preformation is effectively taken into account through the parameters used to calculate the barrier penetration. The preformed cluster model [7–9] either calculate S by solving the Schrödinger equation in charge (mass) asymmetry coordinate or assume some parameterization like $S_L \approx S_\alpha^{(A_L-1)/3}$, where A_L is the mass number of cluster and S_α is the preformation factor for α decay.

In the liquid-drop consideration, the shape parameter is introduced to trace the evolution from the mother nucleus to dinuclear-like system. This evolution is usually assumed to proceed in the coordinate describing the elongation of the system. However, the formation of cluster configuration can also occur in charge (mass) asymmetry coordinate as shown in Refs. [10,11]. The liquid-drop consideration of cluster decay was improved by adding the shell effects in Ref. [12] and considering the tunneling via quasimolecular shapes. A simple formula was derived [9] for calculating cluster decay half-lives using only one adjustable parameter S_α.

In the fragmentation theory [10,11,13,14], the Schrödinger equation was solved to find the probabilities of formation of cluster configurations. An important step of this approach is to calculate properly the potential energy and inertia parameters. If we assume the cluster configuration to be identical to the dinuclear system (DNS), one can use the achievements of the DNS model [15–18] and consider the DNS motion in charge (mass) asymmetry coordinate to find the preformation factor. The decay of the cluster configurations close to symmetry is equivalent to the fission. So, the DNS approach allows us to consider simultaneously the CR and SF.

The model presented here belongs to the cluster type [15–24]. As assumed, the ground state of the nucleus has a small admixture of the cluster-state components [25–30]. In Refs. [15,16], a good description of the CR has been achieved. The next step is to check if our model is able to describe the SF. The problem has to be solved is the calculations of spectroscopic factors and partial half-lives of nuclei with respect to the emission of various clusters. In Refs. [31,32], the microscopic cluster model was applied to produce four-nucleon correlation on the nuclear surface. The shell model was used in Refs. [33–36] to calculate the α-decay width. However, an application of this model to the SF seems to be cumbersome. The relation between the shell model and the cluster model was discussed in Ref. [37]. Recent analysis of experimental data both within the shell model [38,39] and within the cluster model [40] show the importance of shell-like cluster structure in nuclei [41–45]. This means the importance of the microscopic effects in the DNS.

II. MODEL

The process of cluster formation with charge number $Z_L \geqslant 2$ can be described as an evolution of the system in the collective coordinates of the charge asymmetry,

$$\eta_Z = \frac{Z_H - Z_L}{Z_H + Z_L}, \tag{1}$$

and relative separation R of the cluster centers of mass. Here Z_i (A_i), where $i = L, H$, is the charge (mass) number of the ith cluster and $Z = Z_L + Z_H$ ($A = A_L + A_H$) are the total charge (mass) number of the DNS. The mass asymmetry coordinate $\eta = \frac{A_H - A_L}{A_H + A_L}$ is assumed to be strongly related to η_Z by the condition of the potential energy minimum. Though the consideration of η_Z and η as independent variables is possible, the firm relation imposed between these variables is supported

 ©2019 American Physical Society

by the experimental data and allows us to simplify treatment significantly.

A DNS [30] with any η_Z is presented in the ground state of the nucleus with a certain probability which depends on the DNS potential energy with respect to the mother nucleus. Such a DNS decays via tunneling through the barrier of the nucleus-nucleus potential. In the first approximation, the CR or SF can be divided into two independent stages, that are the DNS formation, which is the result of motion in η_Z (η), and the DNS decay in the coordinate R. Therefore, the decay width in the certain channel is proportional to the product of the probability S_L of the DNS formation and the probability of decay of this DNS.

The determination of S_L requires the solution of the stationary Schrödinger equation:

$$H\Psi(\eta_Z) = E\Psi(\eta_Z), \tag{2}$$

where the collective Hamiltonian

$$H = -\frac{\hbar^2}{2}\frac{\partial}{\partial\eta_Z}(B^{-1})_{\eta_Z}\frac{\partial}{\partial\eta_Z} + U(R,\eta_Z,\Omega), \tag{3}$$

contains the inertia coefficient $(B^{-1})_{\eta_Z}$ and the potential energy $U(R,\eta_Z,\Omega)$. So, to find S_L, one should determine the DNS potential energy and DNS mass parameters as functions of η_Z and R.

A. Potential energy of DNS

The potential of DNS [46],

$$U(R,\eta_Z,\Omega) = V(R,\eta_Z,\Omega) - (B - B_L - B_H), \tag{4}$$

is referred to a driving potential. Here B is the mass excess of the mother nucleus and B_L, B_H are the mass excesses of the nuclei forming the DNS considered. The potential energy (4) is normalized with respect to the potential energy of the mother nucleus.

The nucleus-nucleus interaction potential V is represented as the sum:

$$V(R,\eta_Z,\Omega) = V_C(R,\eta_Z) + V_N(R,\eta_Z) + V_r(R,\eta_Z,\Omega), \tag{5}$$

of the Coulomb V_C, nuclear V_N, and centrifugal $V_r = \hbar^2\Omega(\Omega+1)/(2\Im)$ [where $\Im$ is the moment of inertia of the DNS] potentials. Here, we consider the decays of even-even nuclei in the case of zero orbital angular momentum Ω.

The Coulomb potential V_C is calculated as follows:

$$V_C = \frac{e^2 Z_L Z_H}{R}\left\{1 + \frac{3}{5R^2}\sum_{i=L,H} R_i^2\beta_{2i}Y_{20}(\theta_i) + \frac{12}{35R^2}\sum_{i=L,H}[R_i\beta_{2i}Y_{20}(\theta_i)]^2\right\}, \tag{6}$$

where β_{2i} are the parameters of quadrupole deformation. In our calculations, we employed the experimental values of B_L and B_H from Ref. [47] and the values of the quadrupole deformation parameters from Ref. [48]. If the relevant experimental data were not available, we took the calculated values from Ref. [49]. The shape of each cluster is described as

$$R_i(\theta) = r_{0i}A_i^{1/3}[1 + \beta_{2i}Y_{20}(\theta)].$$

Because the mode which is responsible for N/Z equilibrium in the DNS is rather fast, the potential energy U was minimized in η for each fixed value of η_Z.

The nuclear part V_N of the interaction potential is calculated in the double folding form:

$$V_N = \int \rho_H(\boldsymbol{r}_H)\rho_L(\boldsymbol{R}-\boldsymbol{r}_L)F(\boldsymbol{r}_H-\boldsymbol{r}_L)d\boldsymbol{r}_H d\boldsymbol{r}_L, \tag{7}$$

where the density-dependent nucleon-nucleon forces

$$F(\boldsymbol{r}_H-\boldsymbol{r}_L) = C_0\left\{F_{\rm in}\frac{\rho(\boldsymbol{r}_H)}{\rho_0} + F_{\rm ex}\left[1-\frac{\rho(\boldsymbol{r}_H)}{\rho_0}\right]\right\}\delta(\boldsymbol{r}_H-\boldsymbol{r}_L)$$

are folded with the nucleon densities $\rho_H(\boldsymbol{r}_H)$ and $\rho_L(\boldsymbol{R}-\boldsymbol{r}_H)$. Here

$$F_{\rm in,ex} = \xi_{\rm in,ex} + \xi'_{\rm in,ex}\frac{A_L-2Z_L}{A_L}\frac{A_H-2Z_H}{A_H}$$

and $\rho(\mathbf{r}_H) = \rho_H(\mathbf{r}_H) + \rho_L(\mathbf{R}-\mathbf{r}_L)$. The constants $\xi_{\rm in} = 0.09$, $\xi_{\rm ex} = -2.59$, $\xi'_{\rm in} = 0.42$, $\xi'_{\rm ex} = 0.54$, $C_0 = 300$ MeV fm^3 are from Ref. [50]. We take the spatial axial symmetric nucleon density in the form

$$\rho_{L,H}(\mathbf{r}) = \frac{\rho_0}{1+\exp(|\mathbf{r}-\mathbf{R}_{L,H}|/a_{L,H})}, \tag{8}$$

where $\rho_0 = 0.17\,{\rm fm}^{-3}$ and $a_{L,H}$ stands for the diffuseness parameters of the nuclei in the DNS. The values employed in our calculations fell within the range $r_{0L,0H} = 1.0$–1.16 fm for the nuclear radii $R_{L,H} = r_{0L,0H}A_{L,H}^{1/3}$ and within the range $a_{L,H} = 0.47$–0.56 fm for the diffuseness parameters, depending on nuclear mass.

In Fig. 1, the calculated nucleus-nucleus potential $V(R,\eta_Z,\Omega=0)$ is shown for the pole-pole orientation in the ^{24}Ne + ^{208}Pb system. There is a local minimum in this potential at R_0 corresponding to about 0.5 fm between the nuclear surfaces, $V(R_0(\eta_Z),\eta_Z,\Omega=0) = V_0$. The value of

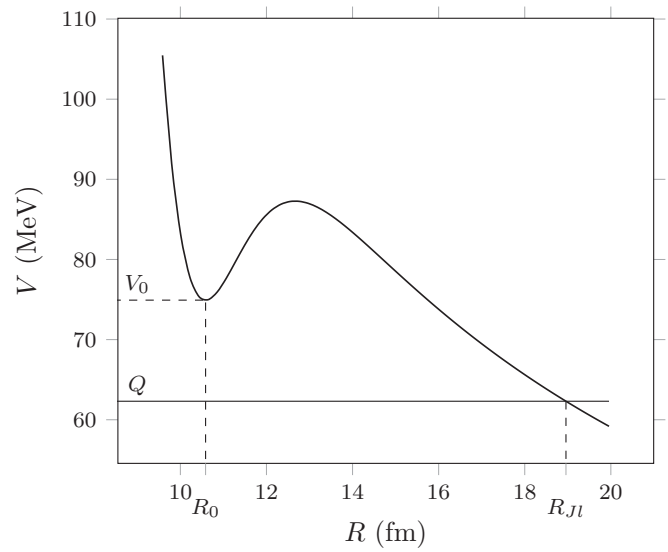

FIG. 1. Calculated nucleus-nucleus potential for the ^{24}Ne + ^{208}Pb system. The bottom of the potential pocket corresponds to V_0 at $R = R_0$. The position of external turning point corresponding to $V = Q$ is shown as R_{JL}.

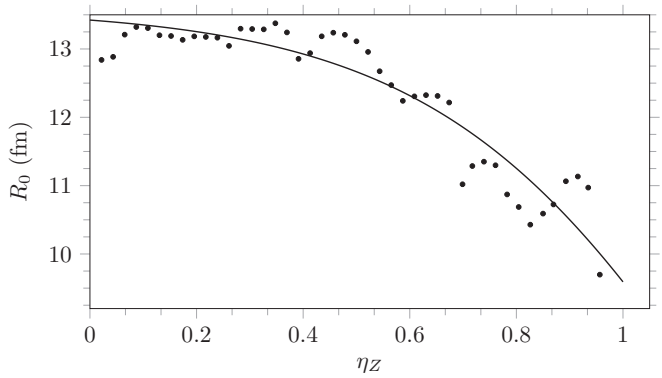

FIG. 2. Calculated contact distance $R = R_0(\eta_Z)$ (dots) of the DNS nuclei versus charge asymmetry coordinate in the system ^{234}U. The solid line is a guide to the eye.

a contact distance R_0 in the DNS depends of η_Z and deformations of nuclei. The decay process is represented as moving the system in R and η_Z coordinates (Fig. 2). The smallest value of R_0 achieves at $\eta_Z = 1$, which corresponds to the mononucleus and represents its size. Generally, the distance R_0 increases with more symmetrical configuration formation. The formation of cluster configurations or DNS with η_Z occurs at $R = R_0(\eta_Z)$. Motion to $R > R_0$ can result in the decay if the DNS escapes the potential pocket in the nucleus-nucleus potential.

B. Inertia parameter

Because of the small overlap of nucleon density profiles in the DNS, the inertia parameter for motion in R is well approximated by the reduced mass $\mu(\eta_Z)$. For the calculation of the mass parameter in η_Z, we use the results of Ref. [51] where the following expression

$$(B^{-1})_{\eta_Z} = \frac{1}{2m_0}\frac{A_{\rm neck}}{2\sqrt{2\pi}b^2A^2}, \tag{9}$$

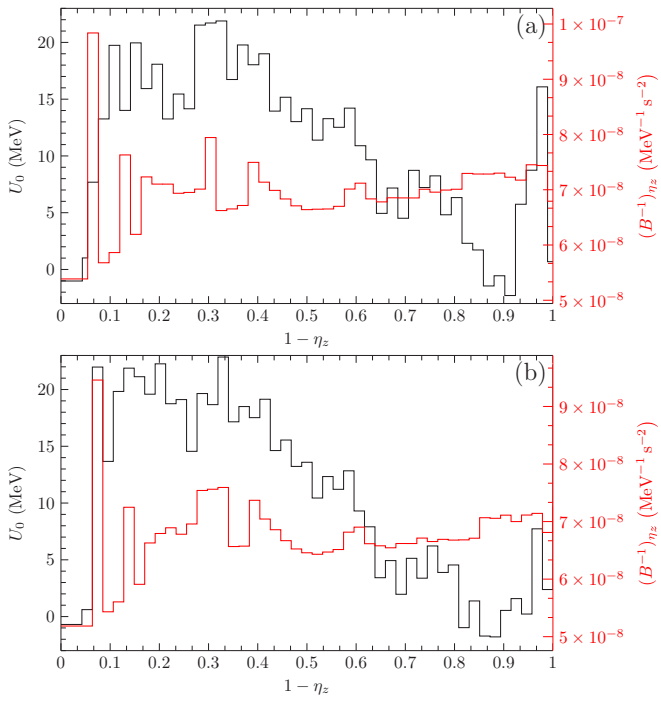

FIG. 3. Calculated driving potential U and inverse mass parameter $(B^{-1})_{\eta_Z}$ as the step functions of x for ^{234}U (a) and ^{238}Pu (b).

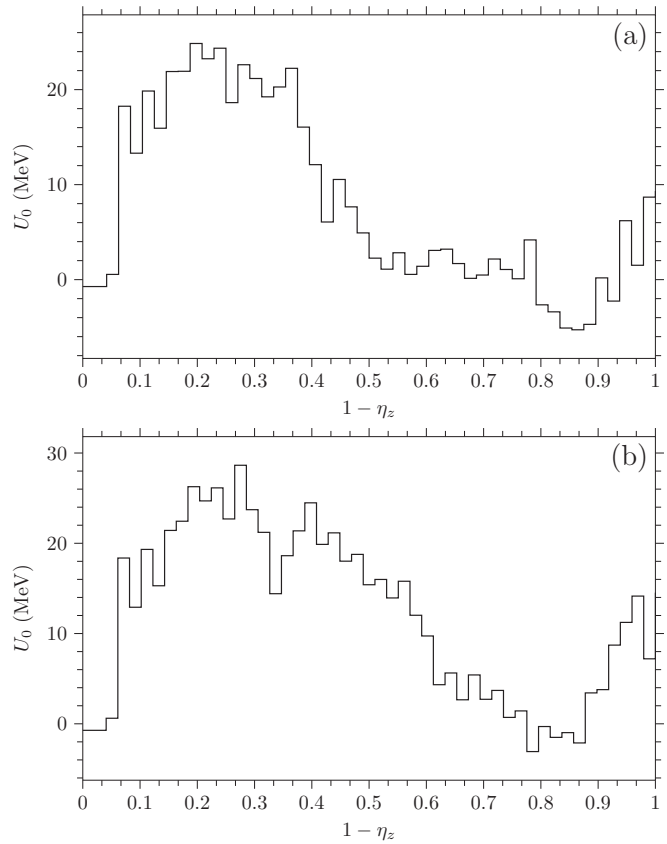

FIG. 4. Calculated driving potential U and as the step function of x for ^{242}Cm (a) and ^{248}Cf (b).

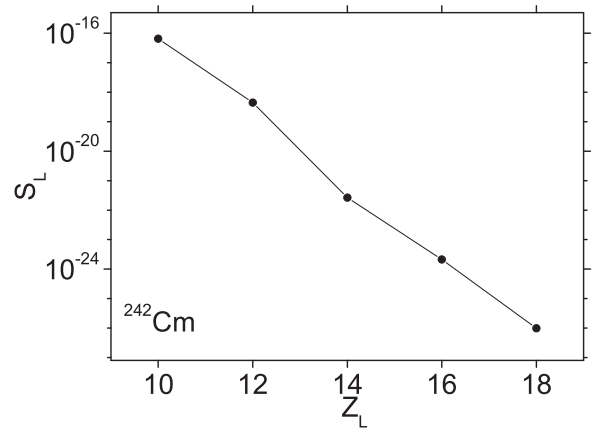

FIG. 5. Calculated spectroscopic factors of the indicated clusters emitted from ^{242}Cm.

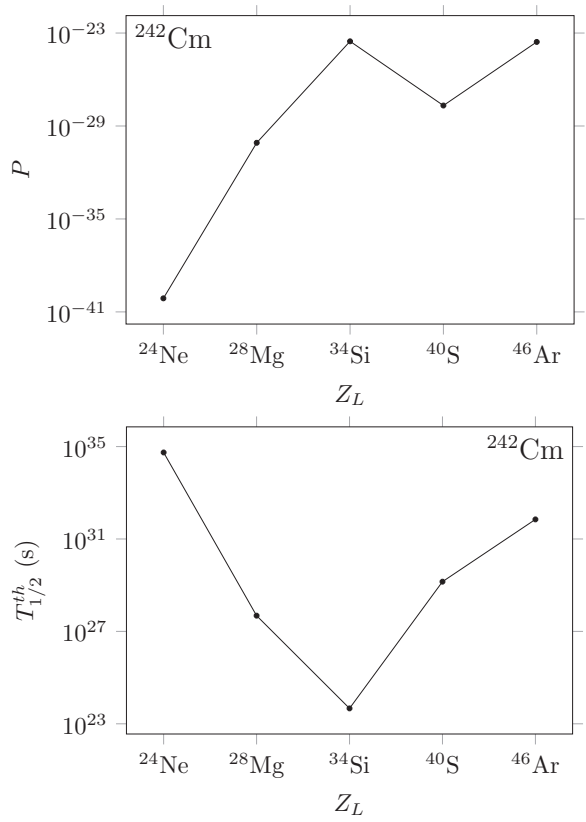

FIG. 6. Calculated penetration probabilities and half-lives of the indicated clusters emitted from ^{242}Cm.

was derived. Here b characterizes the DNS neck size, m_0 is the nucleon mass, and

$$A_{\text{neck}} = \int [\rho_L(\mathbf{r}) + \rho_H(\mathbf{R}-\mathbf{r})] \exp\left(-\frac{z^2}{b^2}\right) d\mathbf{r}$$

is number of nucleons in the neck region between two nuclei. In the present calculations, we set the neck parameter $b = 0.479–0.019\eta_Z$ fm which corresponds to about three to five nucleons in the neck region. Slightly larger b for the symmetric DNS reflects a larger number of nucleons in the neck region between two heavy nuclei.

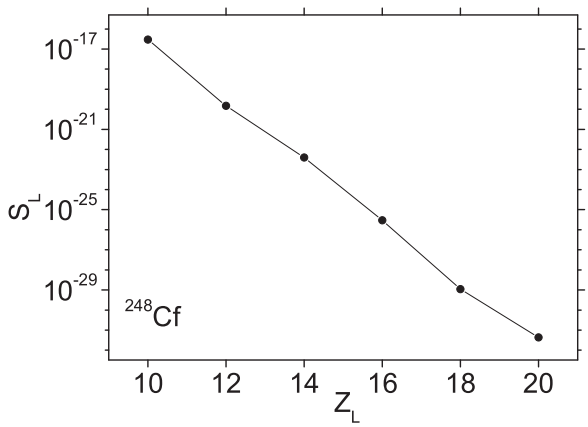

FIG. 7. The same as in Fig. 5 but for ^{248}Cf.

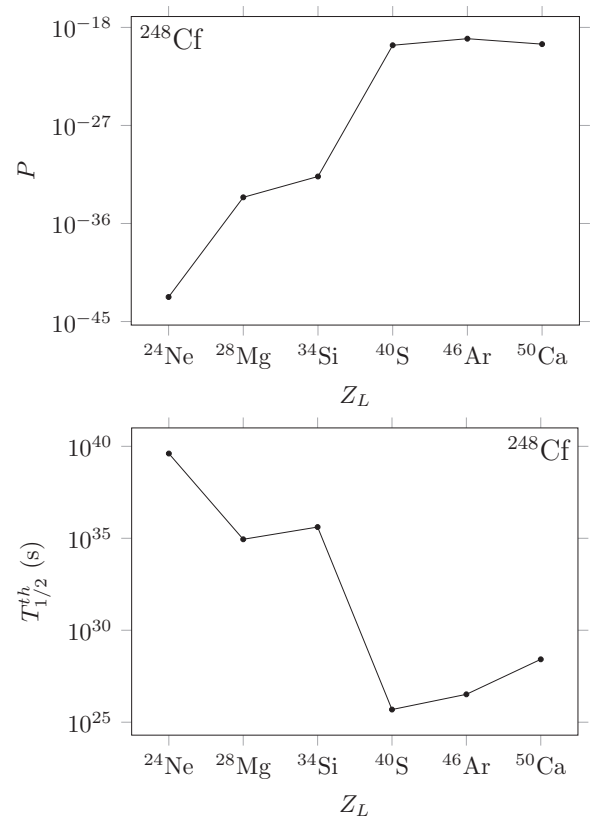

FIG. 8. The same as in Fig. 6, but for ^{248}Cf.

C. Spectroscopic factor

To solve Eq. (2) and find S_L, it is convenient to replace η_Z by

$$x = 2\frac{Z_L}{Z} = 1 - \eta_Z.$$

This replacement of variables preserves the form of Eq. (2) with the function $\Psi(x)$ domain change to $x \in (0, 1)$, where $x = 0$ corresponds to the state of the mononucleus, and $x = 1$ notes the symmetric DNS configuration.

The variable x is discrete by definition and the values of driving potential and inertia parameter are calculated at points $x_L = 2\frac{Z_L}{Z}$. However, the variable x is chosen to be continuous on the interval (0, 1) for solving Eq. (2). Therefore, the values of U and $(B^{-1})_{\eta_Z}$ are extended to the segments of the width $2\Delta = 2/Z$ so that the points $x_{U,B}$ are placed in the middle of the corresponding segments. The only exception is the mononucleus, for which we set $x \in [0, 4\Delta)$ and the α particle with $x \in [4\Delta, 5\Delta]$.

As seen in Figs. 3 and 4, there are local minima of the driving potentials at η_Z close to zero. The potential energies in these minima are smaller than the energy of mononucleus at $\eta_Z = 1$. Thus, the energy resolved configurations appear for the SF. These DNS configurations are excited.

To get the continues functions in Eq. (2), the potential energy and the inertia parameter are approximated with the stepwise functions (Figs. 3 and 4). In this case, Eq. (2) is

TABLE I. Calculated cluster spectroscopic factors S_L for ^{242}Cm and ^{248}Cf.

^{242}Cm		^{248}Cf	
Cluster	S_L	Cluster	S_L
^{4}He	7.96×10^{-04}	^{4}He	1.21×10^{-03}
^{10}Be	3.75×10^{-08}	^{10}Be	1.70×10^{-08}
^{11}B	2.52×10^{-10}	^{11}B	2.66×10^{-10}
^{14}C	1.28×10^{-11}	^{14}C	1.42×10^{-11}
^{15}N	8.36×10^{-12}	^{15}N	9.51×10^{-13}
^{20}O	3.92×10^{-14}	^{20}O	4.21×10^{-14}
^{23}F	1.67×10^{-15}	^{23}F	1.52×10^{-16}
^{24}Ne	6.51×10^{-17}	^{24}Ne	2.95×10^{-17}
^{27}Na	3.14×10^{-18}	^{27}Na	1.61×10^{-19}
^{28}Mg	4.42×10^{-19}	^{28}Mg	1.50×10^{-20}
^{31}Al	3.05×10^{-21}	^{31}Al	7.37×10^{-21}
^{34}Si	2.64×10^{-22}	^{34}Si	3.96×10^{-23}
^{35}P	2.35×10^{-23}	^{39}P	2.81×10^{-24}
^{40}S	2.12×10^{-24}	^{40}S	2.98×10^{-26}
^{41}Cl	3.67×10^{-25}	^{43}Cl	5.16×10^{-28}
^{46}Ar	9.92×10^{-27}	^{46}Ar	1.10×10^{-29}
^{47}K	2.72×10^{-28}	^{47}K	2.15×10^{-30}
^{48}Ca	7.63×10^{-30}	^{50}Ca	4.36×10^{-32}
^{51}Sc	2.0×10^{-30}	^{51}Sc	8.67×10^{-33}
^{56}Ti	5.91×10^{-31}	^{56}Ti	1.70×10^{-34}
^{57}V	1.80×10^{-33}	^{57}V	3.44×10^{-35}
^{58}Cr	5.98×10^{-34}	^{60}Cr	7.60×10^{-36}
^{61}Mn	2.08×10^{-34}	^{61}Mn	1.78×10^{-36}

solved by replacing it by the system of equations

$$-\frac{\hbar^2}{2}\left(B_j^{-1}\right)_{\eta_Z}\frac{\partial^2}{\partial x^2}\psi_j(x) + U_j\psi_j(x) = E\psi_j(x). \quad (10)$$

So Eq. (10) is solved for each interval of x and the functions $\psi_j(x)$ are related to each other by the boundary conditions (see Appendix A).

The wave function is normalized

$$\int_0^1 |\Psi(x)|^2 dx = 1.$$

Using the ground state wave function of Eq. (2), we define the preformation probability S_L of the DNS with certain charge number Z_L of light cluster as follows:

$$S_L = \int_{\eta_Z(Z_L)-\Delta}^{\eta_Z(Z_L)+\Delta} |\Psi(\eta_Z)|^2 d\eta_Z. \quad (11)$$

The products of SF usually correspond to $\eta_Z < 0.3$. Indeed, the potential energies of some DNS configurations with these η_Z are smaller than the potential energy of fissioning mother nucleus. The SF mainly occurs from these configurations. To calculate the SF half-life, one should take all DNS configurations at $\eta_Z < 0.3$ into account by calculating their partial decay widths. In almost symmetric DNS configurations the potential barrier, which keeps the DNS nuclei at contact, is small or absent. In the configurations contributing to SF the DNS excitation usually exceeds the hight of this barrier. So, the decay width of SF is mainly determined by S_L.

TABLE II. Calculated ($T_{1/2}^{\rm th}$) and experimental ($T_{1/2}^{\rm exp}$) α-decay half-lives for even-even U isotopic chain.

	^{232}U	^{234}U	^{236}U
$T_{1/2}^{\rm th}$ (s)	3.021×10^{9}	9.15×10^{12}	9.49×10^{15}
$T_{1/2}^{\rm exp}$ (s) [52]	3.20×10^{9}	7.74×10^{12}	1.00×10^{15}

TABLE III. Calculated ($T_{1/2}^{\rm th}$) and experimental ($T_{1/2}^{\rm exp}$) CR half-lives for even-even U isotopic chain.

	^{232}U → ^{24}Ne	^{234}U → ^{26}Ne	^{234}U → ^{28}Mg	^{236}U → ^{30}Mg
$T_{1/2}^{\rm th}$ (s)	4.07×10^{21}	1.29×10^{25}	4.33×10^{25}	1.85×10^{26}
$T_{1/2}^{\rm exp}$ (s) [52]	1.89×10^{21}	1.20×10^{25}	3.47×10^{25}	1.89×10^{26}

D. Half-lives

The value of the spectroscopic factor S_L cannot be directly measured. Only the experimental half-lives $T_{1/2}$ with respect to the CR and SF are available to be compared with the theoretical estimates. Thus, to compare the theoretical $T_{1/2}$ for the CR the probability P_L of penetration through the Coulomb barrier is calculated in the one-dimensional WKB approximation

$$P_L = \left[1 + \exp\left(\frac{2}{\hbar}\int_{R_0}^{R_{Jl}} \sqrt{2\mu\{V[R, \eta_Z(Z_L), \Omega] - Q\}}dR\right)\right]^{-1},$$

where R_0 and R_{Jl} are marked in Fig. 1, Q is the decay energy. The value of $T_{1/2}$ depends on the products $S_L P_L$. So, the decay width Γ_L is calculated as

$$\Gamma_L = \frac{\hbar\omega_0}{\pi} S_L P_L,$$

where ω_0 is the frequency of zero-point vibration in η_z coordinate near the mononucleus state, $\hbar\omega_0$ is equal to the distance between the ground and the first excited state of DNS. Using the formulas presented, the half-lives are calculated as

$$T_{1/2} = \frac{\hbar \ln 2}{\Gamma_L} = \frac{\pi \ln 2}{\omega_0 S_L P_L}. \quad (12)$$

III. CALCULATED RESULTS

The dependence of the spectroscopic factor S_L on the charge (mass) number of cluster was determined by formula (11) and presented in Table I. The spectroscopic factor exhibits a global trend toward a strong decrease as the charge of the cluster grows. For example, for the nucleus ^{242}Cm

TABLE IV. Calculated ($T_{1/2}^{\rm th}$) and experimental ($T_{1/2}^{\rm exp}$) SF half-lives for even-even U isotopic chain.

	^{232}U	^{234}U	^{236}U
$T_{1/2}^{\rm th}$ (s)	7.43×10^{20}	1.61×10^{22}	1.10×10^{23}
$T_{1/2}^{\rm exp}$ (s) [52]	3.73×10^{21}	4.73×10^{23}	6.38×10^{23}

TABLE V. Calculated ($T^{\rm th}_{1/2}$) and experimental ($T^{\rm exp}_{1/2}$) α-decay CR, and SF half-lives for ^{236}Pu.

	^{4}He	^{28}Mg	SF
$T^{\rm th}_{1/2}$ (s)	4.80×10^{8}	2.06×10^{21}	4.24×10^{17}
$T^{\rm exp}_{1/2}$ (s) [52]	1.30×10^{8}	4.67×10^{21}	1.10×10^{17}

(^{248}Cf), the spectroscopic factor of ^{48}Ca (^{50}Ca) is about 26 (28) orders of magnitude smaller than that of ^{4}He. For the considered below nuclei, the value of $\hbar\omega_0$ weakly changes in the interval (1.8–2.1) MeV. In Figs. 5–8 and Table I, we show how the penetration probability and the spectroscopic factor predetermine the half-lives with respect to the emission of different clusters from ^{242}Cm and ^{248}Cf. In the contrast to S_L, the penetration probability P_L globally increases with the charge number of cluster and the interplay between these two factors determines the cluster with the minimum of half-life. As a result of this interplay, the emissions of clusters ^{34}Si and ^{40}S, respectively, from ^{242}Cm and ^{248}Cf have the minimal lifetimes.

To verify the model, the half-lives (12) with respect to α decay, CR, and SF were calculated (Tables II–IV) and compared with the experimental data [52] for even uranium isotopes. A good agreement between the theory and experiment has been obtained. The maximal deviation from the experimental half-lives is within the factor of 6 that is rather good in the present case without special adjustment of the parameters. Here, we consider only the decays of even-even nuclei from their ground states. Simultaneous good description of the CR and SF in ^{232,234,236}U allows us to apply the model to other nuclei (Tables V–VII).

We consider the nuclei ^{236,238}Pu and ^{242}Cm for which the CR is found. As seen in Tables V–VII, the description of α decay and CR is pretty good. The emissions of neighboring clusters ^{28}Mg($T^{\rm th}_{1/2} = 3.18 \times 10^{25}$ s) and ^{30}Mg($T^{\rm th}_{1/2} = 2.79 \times 10^{25}$ s) from ^{238}Pu are predicted. The SF mainly occurs from the DNS configurations corresponding to the minima of the driving potentials (Figs. 3 and 4) at $Z_L = 38$–42. The potential energies of these minima are smaller than the potential energy of mother nucleus. The wave function in η_Z has local maxima in these potential minima. As known, the U, Pu, and Cm isotopes considered have asymmetric mass distributions of fragments of the SF. The lifetime with respect to the SF is also well described for most of the nuclei. The largest difference of about factor of 8 is for ^{238}Pu. However, it is acceptable for the model without adjustment of the parameters which were set the same for all nuclei considered.

TABLE VI. Calculated ($T^{\rm th}_{1/2}$) and experimental ($T^{\rm exp}_{1/2}$) α-decay CR, and SF half-lives for ^{238}Pu.

	^{4}He	^{30}Mg	^{23}Si	SF
$T^{\rm th}_{1/2}$ (s)	1.21×10^{9}	2.79×10^{25}	5.15×10^{25}	1.01×10^{19}
$T^{\rm exp}_{1/2}$ (s) [52]	3.90×10^{9}	5.01×10^{25}	1.99×10^{25}	1.26×10^{18}

TABLE VII. Calculated ($T^{\rm th}_{1/2}$) and experimental ($T^{\rm exp}_{1/2}$) α-decay CR, and SF half-lives for ^{242}Cm.

	^{4}He	^{34}Si	SF
$T^{\rm th}_{1/2}$ (s)	3.49×10^{7}	2.09×10^{23}	2.53×10^{14}
$T^{\rm exp}_{1/2}$ (s) [52]	1.90×10^{7}	1.41×10^{23}	2.32×10^{14}

Besides the good description of half-lives with respect to α decay and SF for ^{248}Cf, we predict CR with the emission of ^{40}S in this nucleus (see Fig. 8 and Table VIII). This is possible candidate for future experiment, which has has a half-life to be measurable with present experimental setups and reasonable branching ratio with respect to α decay. For the comparison, $T^{\rm th}_{1/2}(^{248}{\rm Cf} \rightarrow {}^{40}{\rm S}) = 233 T^{\rm th}_{1/2}(^{242}{\rm Cm} \rightarrow {}^{34}{\rm Si}) = 4.88 \times 10^{25}$ s, $T^{\rm th}_{1/2}(^{248}{\rm Cf} \rightarrow {}^{46}{\rm Ar}) = 3.28 \times 10^{26}$ s, and $T^{\rm th}_{1/2}(^{248}{\rm Cf} \rightarrow {}^{50}{\rm Ca}) = 2.63 \times 10^{28}$ s.

In Fig. 9, we collect the calculated α decay, CR, and SF half-lives as a function of the parent-nucleus charge number Z. As seen, the α-decay and SF half-lives globally decrease with increasing Z. In contrast, the CR half-life increases with the charge number.

IV. SUMMARY

The model was developed to describe simultaneously the α decay, CR, and SF. All these processes were considered as the evolution of the system in the collective coordinates of charge (mass) asymmetry and in the relative distance between the centers of clusters. Calculating the penetrability of the barrier in the nucleus-nucleus potential, the probability of DNS decay in R is taken into consideration. The decays of almost symmetric DNS configurations are attributed to the SF. Indeed, the SF mainly occurs from the DNS configurations with $\eta_Z < 0.3$ and corresponding to the minima of the driving potential.

The calculated half-lives of α decay, CR, and SF for the nuclei ^{232,234,236}U, ^{236,238}Pu, ^{242}Cm, and ^{248}Cf are in a good agreement with available experimental data. In terms of SF half-lives, the model presented describes well the values which differ up to 12 orders of magnitude. So, the basic assumption of the model on the collective coordinate for the CR and SF seems to be correct. The model allows us to predict the $T_{1/2}$ with respect to the CR and SF for future experiments. For example, the CR with the emission of ^{40}S in the ^{248}Cf nucleus was predicted.

TABLE VIII. Calculated ($T^{\rm th}_{1/2}$) and experimental ($T^{\rm exp}_{1/2}$) α-decay, CR, and SF half-lives for ^{248}Cf.

	^{4}He	^{40}S	SF
$T^{\rm th}_{1/2}$ (s)	3.16×10^{7}	4.88×10^{25}	1.96×10^{12}
$T^{\rm exp}_{1/2}$ (s)	3.50×10^{7} [52]		1.29×10^{12} [53]

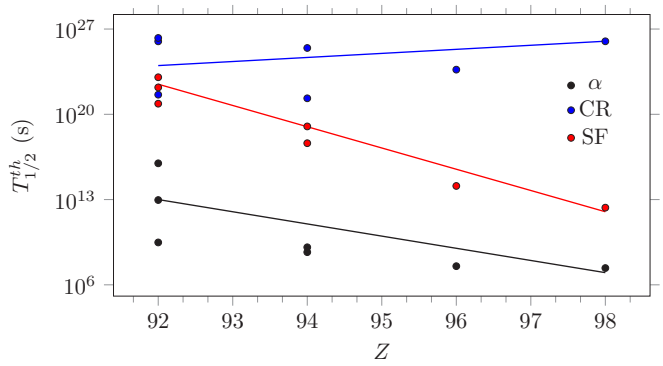

FIG. 9. Calculated (symbols) α-decay, CR, and SF half-lives versus the charge number of the parent nucleus. The solid lines are to guide eye.

ACKNOWLEDGMENTS

This work was partly supported by the RFBR (Moscow), Grant No. 17-52-12015, DFG (Bonn), Contract No. Le439/16, and a Tomsk Polytechnic University Competitiveness Enhancement Program grant.

APPENDIX

The solution of the system of Eqs. (10) in the stepwise potential is the superposition of the plane waves [$j = 0, 1, \ldots, (N-1)$]

$$\psi_j(x) = a_j e^{ik_j x} + b_j e^{-ik_j x};\ k_j = \sqrt{\frac{2}{\hbar^2\left(B_j^{-1}\right)_{\eta_Z}}\left(E - U_j\right)}. \tag{A1}$$

The boundary conditions

$$\left\{\begin{matrix}\psi_j(x_j) = \psi_{j+1}(x_j), \\ \frac{\partial\psi_j(x_j)}{\partial x} = \frac{\partial\psi_{j+1}(x_j)}{\partial x}\end{matrix}\right\}_{j=0,1,\ldots,(N-1)} \tag{A2}$$

for the wave functions at each point x_j provide the continuity of wave functions $\Psi(x)$. The parity conditions

$$\frac{\partial\psi_0(0)}{\partial x} = 0,\ \frac{\partial\psi_N(1)}{\partial x} = 0 \tag{A3}$$

at the borders $x = 0$ and $x = 1$ are taken also into account.

Using (A2) and (A3) in Eqs. (A1), we obtain the complete set of equations

$$a_0 k_0 - b_0 k_0 = 0,$$

$$\left\{\begin{matrix}a_j e^{ik_j x_j} + b_j e^{-ik_j x_j} - a_{j+1} e^{ik_{j+1} x_j} - b_{j+1} e^{-ik_{j+1} x_j} = 0, \\ a_j k_j e^{ik_j x_j} - b_j k_j e^{-ik_j x_j} - a_{j+1} k_{j+1} e^{ik_{j+1} x_j} + b_{j+1} k_{j+1} e^{-ik_{j+1} x_j} = 0,\end{matrix}\right\}_{j=0,1,\ldots,(N-1)} \tag{A4}$$

$$a_N k_N e^{ik_N} - b_N k_N e^{-ik_N} = 0$$

to find the coefficients $\{a_j\}$, $\{b_j\}$. This system of equations can be written in the matrix form:

$$D_e C = 0, \tag{A5}$$

where

$$C = \begin{bmatrix} a_0 \\ b_0 \\ a_1 \\ b_1 \\ . \\ . \\ a_N \\ b_N \end{bmatrix},$$

$$D_e = \begin{bmatrix} k_0 & -k_0 & 0 & 0 & \ldots & 0 \\ e^{ik_0 4\Delta} & e^{-ik_0 4\Delta} & -e^{ik_1 4\Delta} & -e^{-ik_1 4\Delta} & \ldots & 0 \\ k_0 e^{ik_0 4\Delta} & -k_0 e^{-ik_0 4\Delta} & -k_1 e^{ik_1 4\Delta} & k_1 e^{-ik_1 4\Delta} & \ldots & 0 \\ 0 & 0 & e^{ik_1 5\Delta} & e^{-ik_1 5\Delta} & \ldots & 0 \\ 0 & 0 & k_1 e^{ik_1 5\Delta} & -k_1 e^{-ik_1 5\Delta} & \ldots & 0 \\ \ldots & \ldots & \ldots & \ldots & \ldots & \ldots \\ 0 & 0 & 0 & 0 & \ldots & -k_N b_N e^{-ik_N} \end{bmatrix}.$$

Equation (A5) has the solutions in the case of $\det(D_e) = 0$. The energy E of the ground state is set to zero. These two conditions provide the equation

$$\det\left[D_e(E = 0, U_0)\right] = 0$$

for finding the potential energy U_0 of mononucleus.

[1] H. J. Rose and G. A. Jones, Nature **307**, 245 (1984).
[2] D. V. Alexandrov *et al.*, JETP Lett. **40**, 909 (1984).
[3] D. N. Poenaru, M. Ivascu, A. Sandulescu, and W. Greiner, J. Phys. G **10**, L183 (1984).
[4] W. Greiner, M. Ivascu, D. N. Poenaru, and A. Sandulescu, Z. Phys. A **320**, 347 (1985).
[5] G. Royer, R. K. Gupta, and V. Yu. Denisov, Nucl. Phys. A **632**, 275 (1988).
[6] G. Royer and R. Moustabchir, Nucl. Phys. A **683**, 182 (2001).
[7] S. Kumar *et al.*, J. Phys. G **29**, 625 (2003).
[8] M. Balasubramaniam and R. K. Gupta, Phys. Rev. C **60**, 064316 (1999).
[9] A. Zdeb, M. Warda, and K. Pomorski, Phys. Scr. T **154**, 014029 (2013).
[10] H. J. Fink, W. Scheid, and W. Greiner, J. Phys. G **1**, 685 (1975).
[11] H. J. Fink, J. A. Maruhn, W. Scheid, and W. Greiner, Z. Phys. **268**, 321 (1974).
[12] X. J. Bao, H. F. Zhang, B. S. Hu, G. Royer, and J. Q. Li, J. Phys. G **39**, 095103 (2012).
[13] J. A. Maruhn, W. Scheid, and W. Greiner, in *Heavy Ion Collisions*, Vol. 2, edited by R. Bock (North Holland, Amsterdam, 1980), p. 399.
[14] R. K. Gupta, S. Singh, R. K. Puri, and W. Scheid, Phys. Rev. C **47**, 561 (1993).
[15] S. N. Kuklin, G. G. Adamian, and N. V. Antonenko, Yad. Fiz. **68**, 1501 (2005) [Phys. At. Nucl. **68**, 1443 (2005)].
[16] S. N. Kuklin, G. G. Adamian, and N. V. Antonenko, Phys. Rev. C **71**, 014301 (2005).
[17] S. N. Kuklin, G. G. Adamian, and N. V. Antonenko, Yad. Fiz. **71**, 1788 (2008) [Phys. At. Nucl. **71**, 1756 (2008)]; S. N. Kuklin, T. M. Shneidman, G. G. Adamian, and N. V. Antonenko, Eur. Phys. J. A **48**, 112 (2012).
[18] V. V. Volkov, E. A. Cherepanov, and Sh. A. Kalandarov, Phys. Part. Nuclei Lett. **13**, 729 (2016).
[19] Yu. M. Tchuvil'sky, *Cluster Radioactivity* (Moscow State University, Moscow, 1997).
[20] W. Greiner, M. Ivascu, D. N. Poenaru, and A. Sandulescu, in *Treatise on Heavy Ion Science*, edited by D. A. Bromley (Plenum, New York, 1989), Vol. 8, p. 641.
[21] D. N. Poenaru *et al.*, At. Data Nucl. Data Tables **34**, 423 (1986); **48**, 231 (1991).
[22] Yu. S. Zamyatnin *et al.*, Sov. J. Part. Nuclei **21**, 231 (1990).
[23] S. G. Kadmensky, S. D. Kurgalin, and Yu. M. Tchuvil'sky, Phys. Part. Nuclei **38**, 699 (2007).
[24] D. N. Poenaru, *Nuclear Decay Modes* (IOP, Bristol, 1996).
[25] T. M. Shneidman, G. G. Adamian, N. V. Antonenko, R. V. Jolos, and W. Scheid, Phys. Lett. B **526**, 322 (2002); Phys. Rev. C **67**, 014313 (2003).
[26] G. G. Adamian, N. V. Antonenko, R. V. Jolos, and T. M. Shneidman, Phys. Rev. C **70**, 064318 (2004).
[27] G. G. Adamian, N. V. Antonenko, R. V. Jolos, Yu. V. Palchikov, and W. Scheid, Phys. Rev. C **67**, 054303 (2003).
[28] G. G. Adamian, N. V. Antonenko, R. V. Jolos, Yu. V. Palchikov, W. Scheid, and T. M. Shneidman, Phys. Rev. C **69**, 054310 (2004).
[29] T. M. Shneidman, G. G. Adamian, N. V. Antonenko, and R. V. Jolos, Phys. Rev. C **74**, 034316 (2006).
[30] G. G. Adamian, N. V. Antonenko, and W. Scheid, *Clusters in Nuclei*, Vol. 2, Lecture Notes in Physics, Vol. 848, edited by C. Beck (Springer-Verlag, Berlin, 2012), p. 165.
[31] K. Wildermuth, F. Fernandez, E. J. Kanellopoulos, and W. Sünkel, J. Phys. G **6**, 603 (1980).
[32] T. Steimayer, W. Sünkel, and K. Wildermuth, Phys. Lett. B **125**, 437 (1983).
[33] H. J. Mang, Phys. Rev. **119**, 1069 (1960).
[34] T. Fliessbach and H. J. Mang, Nucl. Phys. A **263**, 75 (1976).
[35] F. A. Janouch and R. J. Liotta, Phys. Rev. C **25**, 2123 (1982).
[36] G. Dodig-Crnković, F. A. Janouch R. J. Liotta, and L. J. Sibanda, Nucl. Phys. A **444**, 419 (1985).
[37] K. Varga, R. G. Lovas, and R. J. Liotta, Phys. Rev. Lett. **69**, 37 (1992).
[38] C. Vargas, J. G. Hirsch, P. O. Hess, and J. P. Draayer, Phys. Rev. C **58**, 1488 (1998).
[39] B. Cederwall *et al.*, Nature **469**, 68 (2011).
[40] N. Itagaki, J. Cseh, and M. Ploszajczak, Phys. Rev. C **83**, 014302 (2011).
[41] J. Cseh, A. Algora, J. Darai, and P. O. Hess, Phys. Rev. C **70**, 034311 (2004).
[42] W. Sciani, Y. Otani, A. Lépine-Szily, E. A. Benjamim, L. C. Chamon, R. L. Filho, J. Darai, and J. Cseh, Phys. Rev. C **80**, 034319 (2009).
[43] J. Cseh, J. Darai, W. Sciani, Y. Otani, A. Lépine-Szily, E. A. Benjamim, L. C. Chamon, and R. L. Filho, Phys. Rev. C **80**, 034320 (2009).
[44] D. Lebhertz *et al.*, Phys. Rev. C **85**, 034333 (2012).
[45] A. Algora, J. Cseh, J. Darai, and P. O. Hess, Phys. Lett. B **639**, 451 (2006).
[46] G. G. Adamian *et al.*, Int. J. Mod. Phys. E **5**, 191 (1996).
[47] J. K. Tuli, *Nuclear Wallet Cards* (BNL, New York, 2000).
[48] S. Raman *et al.*, At. Data Nucl. Data Tables **78**, 1 (2001).
[49] P. Möller and J. J. Nix, At. Data Nucl. Data Tables **39**, 213 (1988).
[50] A. B. Migdal, *Theory of Finite Fermi Systems and Applications to Atomic Nuclei* (Nauka, Moscow, 1982; Interscience, New York, 1967).
[51] G. G. Adamian, N. V. Antonenko, and R. V. Jolos, Nucl. Phys. A **584**, 205 (1995).
[52] http://www.nndc.bnl.gov/nndc/ensdf/.
[53] N. K. Skobelev, B. A. Grozdev, and V. A. Druin, At. Energ. USSR **24**, 65 (1968).